

Electrical characterization of single GaN nanowires

This article has been downloaded from IOPscience. Please scroll down to see the full text article.

2005 Nanotechnology 16 2941

(<http://iopscience.iop.org/0957-4484/16/12/037>)

View [the table of contents for this issue](#), or go to the [journal homepage](#) for more

Download details:

IP Address: 203.237.47.24

The article was downloaded on 08/04/2011 at 06:29

Please note that [terms and conditions apply](#).

Electrical characterization of single GaN nanowires

E Stern^{1,7}, G Cheng^{1,7}, E Cimpoiasu², R Klie⁵, S Guthrie⁴,
J Klemic², I Kretzschmar², E Steinlauf³, D Turner-Evans²,
E Broomfield², J Hyland², R Koudelka², T Boone², M Young²,
A Sanders⁴, R Munden³, T Lee⁶, D Routenberg² and M A Reed^{2,3,4}

¹ Department of Biomedical Engineering, Yale University, New Haven, CT 06520, USA

² Department of Electrical Engineering, Yale University, New Haven, CT 06520, USA

³ Department of Applied Physics, Yale University, New Haven, CT 06520, USA

⁴ Department of Physics, Yale University, New Haven, CT 06520, USA

⁵ Center for Functional Nanomaterials, Brookhaven National Laboratory, Upton, NY 11973, USA

⁶ Department of Materials Science and Engineering, Gwangju Institute of Science and Technology, Buk-gu, Gwangju 500-712, Korea

E-mail: eric.stern@yale.edu and guosheng.cheng@yale.edu

Received 3 August 2005, in final form 3 October 2005

Published 25 October 2005

Online at stacks.iop.org/Nano/16/2941

Abstract

In this paper a statistically significant study of 1096 individual GaN nanowire (NW) devices is presented. We have correlated the effects of changing growth parameters for hot-wall chemically-vapour-deposited (HW-CVD) NWs fabricated via the vapour–liquid–solid mechanism. We first describe an optical lithographic method for creating Ohmic contacts to NW field effect transistors with both top and bottom electrostatic gates to characterize carrier density and mobility. Multiprobe measurements show that carrier modulation occurs in the channel and is not a contact effect. We then show that NW fabrication runs with nominally identical growth parameters yield similar electrical results across sample populations of >50 devices. By systematically altering the growth parameters we were able to decrease the average carrier concentration for these as-grown GaN NWs ~10-fold, from 2.29×10^{20} to $2.45 \times 10^{19} \text{ cm}^{-3}$, and successfully elucidate the parameters that exert the strongest influence on wire quality. Furthermore, this study shows that nitrogen vacancies, and not oxygen impurities, are the dominant intrinsic dopant in HW-CVD GaN NWs.

1. Introduction

Semiconducting crystals grown by highly anisotropic, unidirectional methods have been known since the pioneering works of Wagner *et al* [1] and Hiruma *et al* [2], and are a subject of intense contemporary interest [3–7] because they represent the limit of semiconductor crystalline solids. These structures, termed nanowires (NWs), are typically single-crystal, solid cylindrical structures nanometres in diameter and microns in length and can be synthesized from a vast array of traditional semiconducting materials. GaN is of particular interest because of its optoelectronic properties and because it

has been shown to yield good quality NWs [8] and can be either grown intrinsically n-type or doped p-type by the incorporation of magnesium during growth [9].

Single-nanowire field effect transistors (FETs) are realized by defining at least two metallic contacts leading to interconnections, which form the source and drain, with either a fabricated top-gate or a buried substrate back-gate. Since there are currently no suitable high-throughput NW-to-individually-addressable-interconnect alignment techniques, electron-beam (e-beam) lithography is often the method of choice to define contacts due to its ability to create custom patterns. However, this serial method is impractical for obtaining statistically significant data on the electrical

⁷ Authors to whom any correspondence should be addressed.

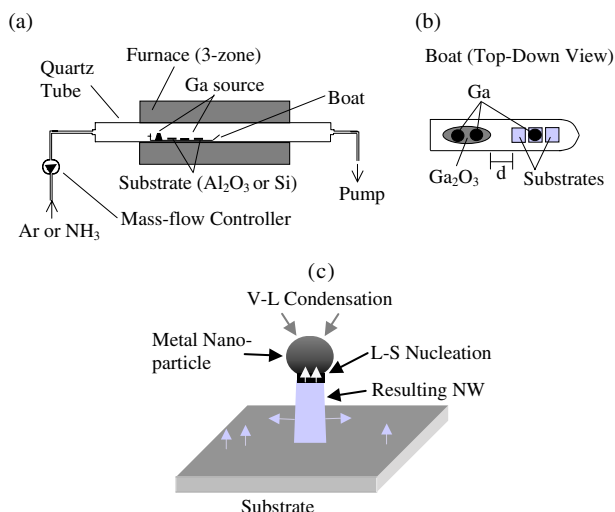


Figure 1. (a) Schematic of the hot wall growth tube furnace showing two substrates and the solid gallium source in the boat within the quartz tube. During growth the tube is sealed and connected to a pump, and ammonia enters through a mass-flow controller. (b) A top-down view of the boat depicting the relative location of samples and gallium sources in the alumina boat; the black circles represent elemental gallium and the dark grey area oval represents Ga_2O_3 powder (for growths in which it is included). The elemental gallium residing between the substrates sits on a silicon wafer chip identical to the substrates but which is discarded when the growth is completed. When alumina discs are used they stand on edge facing the elemental gallium between them. The distance d between the source and the substrates labelled in the schematic diagram is $\sim 1\text{--}10$ mm; the distance between substrates is $\sim 1\text{--}5$ mm. (c) Schematic diagram depicting the suggested VLS growth mechanism. Gallium and ammonia vapour condense in the molten Ni or Fe nanoparticle (VL condensation) and crystallize at the substrate (LS nucleation).

(This figure is in colour only in the electronic version)

properties of NWs. A more practical method is a parallel technique such as optical lithography to define electrodes.

A study containing a statistically significant number of devices is crucial to understanding NW material and device properties since interdevice fluctuations can be pronounced at the nanoscale. Additionally, contact phenomena can confound the analysis since the devices and contacts are of comparable length scales. To date, no study has either attempted to quantify these fluctuations or reported a statistically significant sample size sufficient for correlations with material synthesis parameters. This study presents such a sample, and in addition eliminates systematic errors due to biased NW selection: in contrast to the preselection inherent in e-beam processing, optically defined interconnects randomly contact dispersed NWs. Furthermore, a multitude of devices are fabricated in one exposure, eliminating process fluctuations or systematic errors inherent in a serial approach. Thus a parallel fabrication approach within an appropriate NW density regime and with suitable controls should allow one to determine significant materials parameters and iteratively improve synthesis.

2. Experimental methods

The GaN NWs used for these studies are grown by the supposed vapour–liquid–solid mechanism [10] in a hot-wall

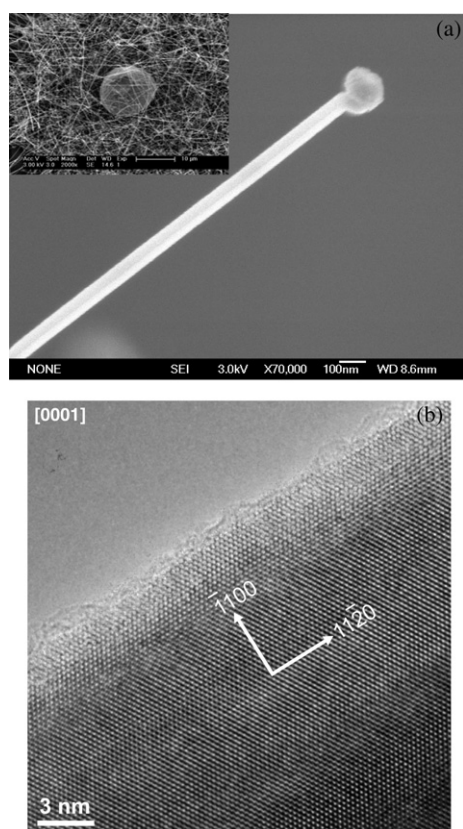
chemical vapour deposition (HW-CVD) system, shown in figure 1(a). Samples for this study were grown on either an alumina (Alfa Aesar) or native SiO_2 on silicon (Silicon Quest International) substrate coated with a 20–50 Å-thick Ni (Kurt J Lesker Co., 99.9995%) or Fe (Kurt J Lesker Co., 99.95+%) catalyst deposited using an e-beam evaporator. Prior to catalyst evaporation, the alumina and silicon substrates are cleaned with a 10 min sonication in VLSI-grade acetone and methanol (100%, Brand-Nu Laboratories) followed by an 80 °C bake. During catalyst evaporation, samples are rotated to improve film uniformity. It has been found that catalyst thickness has a negligible effect on NW electronic parameters, though thicker catalysts tend to produce NWs in higher yield. After film deposition samples are again cleaned in acetone and methanol with sonication and baked.

The schematic diagram in figure 1(a) shows the furnace (Mellen 3-zone 1200 °C furnace) with substrates loaded and the solid gallium source in the alumina boat within the quartz tube. The sources, Ga (99.999%, Alfa Aesar) and Ga_2O_3 (99.999%, Alfa Aesar), and substrates are arranged in the boat as shown in the top view schematic diagram, figure 1(b). Depending on the growth, Ga_2O_3 may or may not be included. Alumina substrates are placed on-edge facing the Ga pellet (except for one growth, in which they were positioned flat), while Si chips always lie flat. After inserting the boat the tube is sealed and pump/purged first with ultra-high purity (UHP) argon and second with ammonia (99.999 99%, Air Products) at ambient temperature. The mass-flow controller (MKS model 1479A) for the ammonia, which serves as the source of elemental nitrogen for NW growth, is then set and the temperature is increased to growth temperature. When heated, the thin metal film on the substrate coalesces into molten nanoparticles, each of which serves as an NW growth catalyst, as schematically illustrated in figure 1(c). The catalytic vapour–liquid–solid (VLS) growth mechanism assumed here (note that alternative growth modes can exist [11] in other systems and under different growth regimes) has gallium vapour from the solid source and nitrogen produced by the cracking of ammonia dissolving into the metal (vapour–liquid condensation), with crystal growth nucleating at the substrate and proceeding upwards (liquid–solid nucleation). A mixture of elemental Ga and its oxide is predominantly used as the gallium source because it has been found that oxide-assisted growth produces a higher NW yield in the NW-CVD system [12]. The SEM image in figure 2(a) shows an NW with the attached catalyst at the end. After the furnace is cooled to ambient temperature, the substrate with NWs is removed from the furnace for further processing. When growth is complete, the NWs lie clustered together on the substrate, figure 2(a). High-resolution TEM studies show a representative NW from a growth with nominally identical parameters to growth A (see table 1) to be single-crystal, hexagonal wurtzite GaN (figure 2(b)). This image indicates that the amorphous oxide layer coating the NW is thin, typically two or three atomic layers.

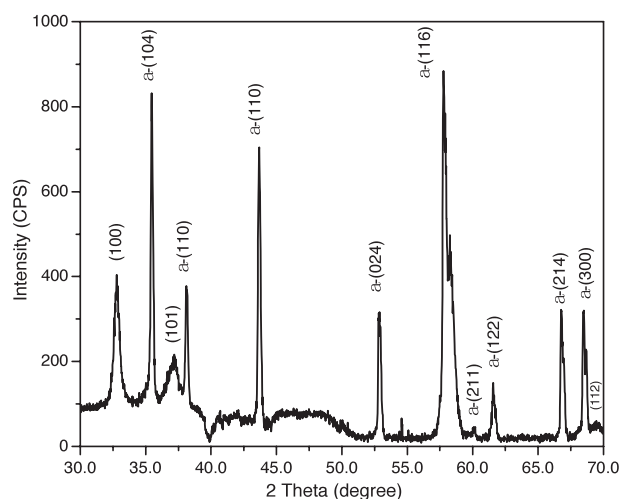
X-ray diffraction (XRD) was performed on representative GaN NWs (growth E) on their alumina growth substrate. Figure 3 shows a typical 2θ XRD spectra of a GaN NW sample, illustrating peaks from both the NW sample and the substrate. The peaks labelled without an ‘a-’ prefix are

Table 1. Material synthesis variables used in the HW-CVD GaN NW study. The sample ID corresponds to distinct growth runs (with the exception of R–S and T–U, which were grown together but annealed under different conditions).

ID	# dev	Sub.	T ($^{\circ}\text{C}$)	P (Torr)	Ga source	NH_3	Catalyst	Anneal
A	59	Alumina	900	760	Mix	100	Ni	No
B	68	Silicon	900	760	Mix	100	Ni	No
C	34	Alumina	900	760	Mix	100	Ni	No
D	59	Alumina	800	760	Mix	100	Ni	No
E	103	Alumina	800	760	Mix	100	Ni	No
F	92	Alumina	800	760	Mix	150	Ni	No
G	53	Alumina	800	760	Mix	50	Ni	No
H	78	Alumina	800	760	Mix	5	Ni	No
I	36	Alumina	900	760	Ga only	100	Ni	No
J	69	Silicon	800	760	Mix	100	Ni	No
K	33	Silicon	1000	760	Mix	100	Ni	No
L	50	Silicon	1100	760	Mix	100	Ni	No
M	60	Alumina	850	760	Mix	100	Fe	No
N	37	Silicon	900	300	Mix	100	Fe	No
O	83	Alumina	850	760	Mix	100	Ni	No
P	44	Alumina	950	760	Mix	100	Fe	No
Q	19	Alumina	950	760	Ga only	100	Fe	No
R	33	Silicon	900	760	Mix	100	Ni	4 h, 900 $^{\circ}\text{C}$ NH_3
S	16	Silicon	900	760	Mix	100	Ni	4 h, 900 $^{\circ}\text{C}$ FG
T	28	Silicon	900	760	Mix	2	Fe	No
U	42	Silicon	900	760	Mix	2	Fe	4 h, 900 $^{\circ}\text{C}$ NH_3

**Figure 2.** (a) SEM image of one GaN NW with the attached Ni catalyst. The inset shows a cluster of NWs on the growth substrate at lower magnification (the ball in the centre is a Ga pellet). (b) A high-resolution 300 keV TEM image of one GaN NW. A thin amorphous oxide layer is seen on the outer surface. This wire has grown in the 1120 direction and is single-crystal hexagonal wurtzite.

indexed as hexagonal wurtzite GaN (space group: $P63mc$) with primitive cell parameters at $a_0 = 3.186 \text{ \AA}$ and $c_0 =$

**Figure 3.** Room-temperature x-ray diffraction pattern (XRD) of GaN nanowires on an alumina substrate. The peaks labelled without the ‘a-’ prefix are indexed as hexagonal wurtzite GaN (space group $P63mc$) with primitive cell parameters at $a_0 = 3.186 \text{ \AA}$ and $c_0 = 5.178 \text{ \AA}$. Those with an ‘a-’ prefix are interpreted as the substrate of rhombohedral $\alpha\text{-Al}_2\text{O}_3$ with primitive cell parameters $a = 4.758 \text{ \AA}$ and $c = 12.991 \text{ \AA}$.

5.178 \AA , in good agreement with the HRTEM results. The peaks with ‘a-’ prefixed indices are interpreted as the substrate of rhombohedral $\alpha\text{-Al}_2\text{O}_3$ with primitive cell parameters at $a = 4.758 \text{ \AA}$ and $c = 12.991 \text{ \AA}$.

The growth conditions for the 21 NW fabrication runs discussed in this paper, labelled A–U, are tabulated in table 1. The six growth variables studied are the following.

- (1) Growth substrate: alumina or Si.
- (2) Growth temperature: varied from 800 to 1100 $^{\circ}\text{C}$, the extremes for NW growth with sufficient yield.

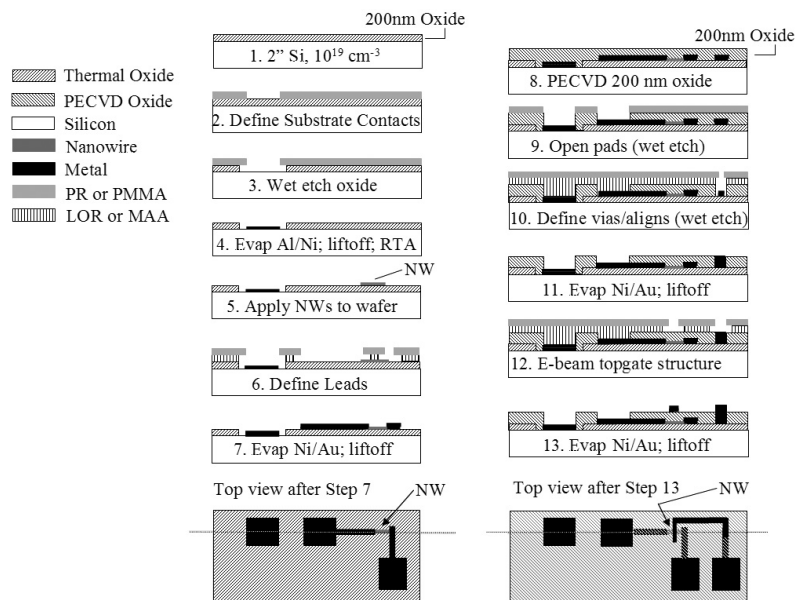


Figure 4. Cross-sectional schematic diagram of the NW device process flow. The main process comprises steps 1–7; steps 8–13 are performed uniquely for top-gate definition. Top views are shown for the device after steps 7 and 13. The above geometry is shown for schematic purposes only; the actual device layout deviates slightly. The alignment marks defined in step 10 are not shown but are necessary for proper top-gate alignment in step 12.

- (3) Growth pressure: varied in a small range from 760 to 300 Torr.
- (4) The gallium source: altered by either including or excluding Ga_2O_3 .
- (5) The ammonia flow rate: varied from 5 to 150 sccm.
- (6) The catalyst: Ni or Fe.

In addition, for some growths a post-growth, pre-lithographic fabrication anneal at 900°C for 4 h in either forming gas (4% hydrogen in nitrogen, Air Products, UHP) or ammonia was performed; higher annealing temperatures were found to be destructive to the wires. Catalyst film thickness and source–substrate distance are not considered in this study because they were each found to solely affect NW yield.

The processing steps for device fabrication are outlined in figure 4. Starting with a 2-inch n^{++} or p^{++} (10^{19} cm^{-3}) doped silicon wafer with a 200 nm thermal oxide (Silicon Quest International), positive photoresist (S1813, Shipley) is used for back-gate definition. After an exposure with a transparency mask (CAD Art Services, Inc.) and development (MF312, MicroChem), the wafer is etched in 6:1 buffered hydrofluoric acid (BHF, Brand-Nu Laboratories) and metallized with a 50 nm Al (99.999%, Kurt J Lesker)/10 nm Ni stack using an e-beam evaporator. Lift-off is then performed at room temperature in acetone with sonication. The wafers are then rapid-thermal-annealed (Heatpulse 210T-02) at 300°C for 30 s to ensure the substrate contact is Ohmic.

The NWs must then be transferred from their growth substrate to the wafer, achieved by creating an NW suspension in isopropanol (IPA, 100%, Brand-Nu Laboratories) by briefly sonicating the growth substrate in the alcohol for 10–45 s. The suspension is then applied dropwise to the wafer and upon IPA evaporation the NWs adhere to the oxide surface across the wafer in a random dispersion. The NWs have been found to strongly adhere to the wafer—sonication and etching are the

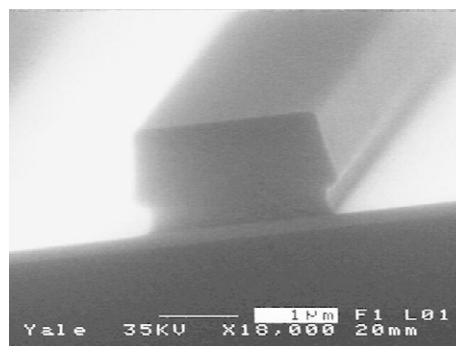


Figure 5. Edge-on SEM image of the LOR/S1813 bilayer resist profile used for lift-off metallization.

only successful removal methods. A second optical step is now performed to contact the NWs. Thin lines 2 or 3 μm wide spaced 2 or 3 μm apart, respectively, run parallel for $\sim 1 \text{ mm}$ before fanning out to contact pads. Adjacent metal leads are electrically isolated unless linked by an NW. The limitations of this process are that the wires must be at least $\sim 3 \mu\text{m}$ long to span the leads and that the wire density must be high enough to obtain devices yet low enough to minimize multiple-NW devices. Samples with low NW yields can often be successfully fabricated by applying multiple drops of the NW suspension to the wafer.

Since subjecting the NWs to metal etchants is highly undesirable, contacts are deposited with a lift-off metallization. In order to create the lift-off profile required for this process we use a resist bilayer consisting of a lift-off resist (LOR, MicroChem) that develops anisotropically and S1813 photoresist (figure 5). The resist is exposed with a chrome mask (Benchmark Technologies) and developed as before. Prior to evaporation, organic residue in the developed areas is

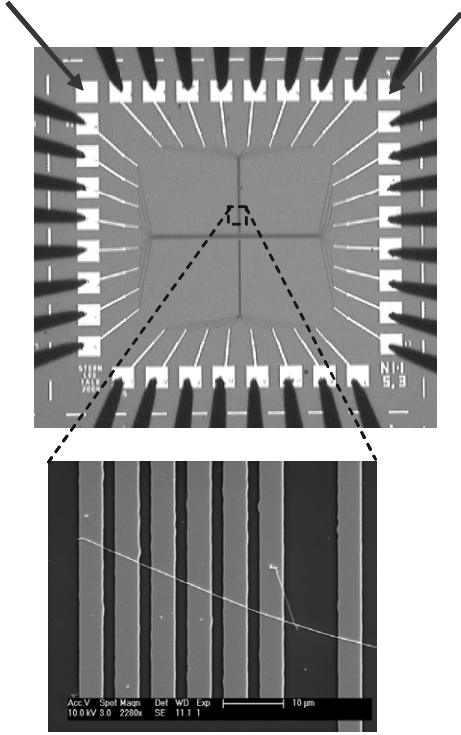


Figure 6. Optical micrograph of a typical die (3.333 mm²). Arrows denote the pads contacting the substrate back-gate. The die is shown contacted by 33 probe tips of a Cascade Microsystems Autoprobstation, used for automated device screening. A scanning electron micrograph highlights a GaN NW contacted by 7 leads.

removed using an oxygen plasma, achieved with a GaSonic Aura 2000 asher. We have observed that this step is crucial to creating unannealed Ohmic contacts to the NWs [14]. A 50 nm Ni/200 nm Au (99.999%, Cerac) stack is then evaporated and the lift-off is performed in 1-methyl-2-pyrrolidinone (NMP, 99.9%, Brand-Nu Labs) at 60 °C without sonication. This creates the metal pattern seen in the optical micrograph in figure 6, which randomly contacts the NWs as illustrated in the scanning electron micrograph. Nickel is used because it has been shown to contact n-type GaN NWs [9]; gold is chosen because of its high conductivity and the ease of wire-bonding.

A Cascade Microtech Autoprobstation controlled by a custom LabView (National Instruments) program is used to electrically characterize every adjacent metallization configuration, and to automatically iterate through each of the ~150 dies (per wafer). An Agilent Technologies Switchbox multiplexes the appropriate lead configurations, and the configuration is measured with an Agilent 5146B semiconductor parameter analyser. The DC current noise-floor for this system is ~50 fA and the pad-to-pad isolation is ~100 pS. Typical zero-bias conductance values for n-type GaN devices range from ~1 mS to ~10 nS. After a full wafer scan to screen for candidate devices, leads with Ohmic contacts to wires are revisited and $I_{SD}(V_{SD})$ sweeps are taken while varying V_{GD} . For this study, ‘Ohmic contacts’ are defined as devices with $I_{SD}(V_{SD})$ plots with a linear best-fit correlation coefficient $R^2 > 0.99$. Schottky contacts are occasionally observed, occurring ~5–10% of the time, and are not included in the study. It should be noted that for these NWs no post-

metallization anneal is required, so Ohmic contact percentage yield could be improved; however, the ability to create Ohmics without annealing allows one to eliminate any systematic errors on material properties due to thermal effects.

Two-point measurements were made by varying the voltage and measuring current; four-point measurements were made by sweeping a current across the outer leads and measuring the voltage across the inner leads. Two-point measurements are made for the inner electrodes of the four-point contact, and resistance values are defined as the inverse of the best-fit linear approximation to the $I_{SD}(V_{SD})$ plot. $I_{SD}(V_{SD}, V_{GD})$ characteristics have occasionally been checked by both two-point and four-point measurements and no difference is observed.

The transconductance of the device is calculated by the linear best fit to the $I_{SD}(V_{GD})$ dependence. The capacitance is calculated using the measured geometrical parameters. To calculate carrier mobility, it is observed that few of the devices at this carrier density saturate over the range of accessible source–drain bias voltage, and thus a mobility is reported by choosing a constant source–drain voltage (here, $V_{SD} = 1$ V) for consistency. Thus, we calculate mobility and carrier density according to

$$\mu = \left(\frac{C}{L^2} V_{SD} \right)^{-1} \left. \frac{\partial I_{SD}}{\partial V_{GD}} \right|_{V_{SD}=1}, \quad (1)$$

where $C = \frac{2\pi\epsilon\epsilon_0 L}{\ln(4h/d)}$, L is the source–drain NW length, h is the oxide thickness, d is the NW diameter, and

$$n = \frac{\sigma}{e\mu}. \quad (2)$$

Device simulations (Silvaco) quantitatively reproduce the characteristics from the derived mobility, show the suppression of saturation at these mobilities/densities over the accessible source/drain voltages, and verify saturation at lower densities.

The lengths and diameters of the NWs must be known, so these data are obtained by scanning all leads with devices of interest with an FE-SEM (FEI XL-30 ESEM FEG). Further, during this process all devices that are found to consist of multiple NWs are discarded. Diameters are approximated to the nearest 5 nm and lengths to the nearest 0.05 μm .

Typical characterization is achieved by back-gating due to the ease of fabrication, but top-gates were fabricated on some samples to contrast gating efficacy. For this process (figure 4, steps 8–13), a 200 nm thick silicon oxide was deposited by plasma-enhanced chemical vapour deposition (PECVD), performed with a NEXX-Circus 150 system. Wafers were then optically processed to remove the PECVD oxide overlaying the contact pads, achieved with a BHF etch. An MAA EL 13/PMMA 950 A4 (MicroChem) e-beam resist bilayer was then deposited on the wafer. As with the LOR/PR stack for optical processing, this MAA/PMMA stack provides an undercut lift-off profile. Openings were defined above leads not in contact with NWs using a JEOL JSM-6400 SEM with a beam blanked Nabity pattern definition system. Through vias were wet etched into the PECVD oxide with a timed BHF etch followed by an e-beam evaporation of a 10 nm Ni/400 nm Au stack. Alignment marks for the subsequent e-beam fabrication step were also defined in this process step. Lift-off is performed

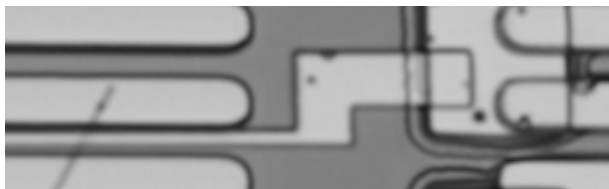


Figure 7. Optical micrograph of an e-beam defined top-gate structure above a 200 nm PECVD oxide deposited on an optically contacted NW device. The NW is visible on the left as a thin black line inclined at $\sim 30^\circ$ from the vertical, with source/drain leads the wide (overlying) top and bottom metal leads, and the gate the centre thin metal line. The gate lies above a PECVD oxide. The gate lead contacts the box on the right, a metallized via through the PECVD oxide that connects the gate to the two redundant leads on the right.

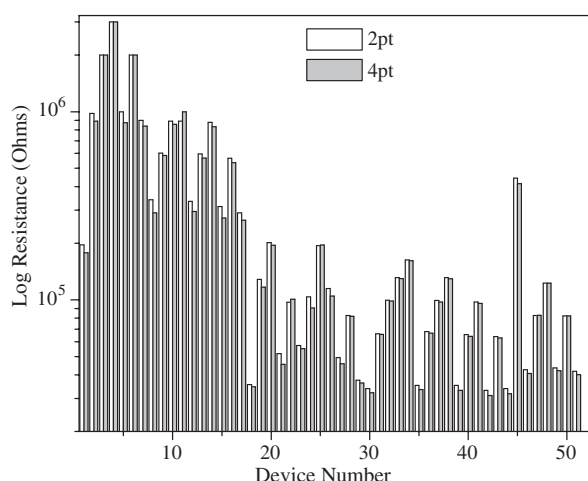


Figure 8. Comparison of two-point and four-point zero-bias device resistances for 51 devices. The average percentage error of the two points relative to the four points is 4.9%.

in boiling acetone without sonication and, upon completion, wafers were again prepared with the MAA/PMMA stack. Top-gates were then defined over NW devices between the contacting leads by e-beam exposure; alignment was achieved using the marks defined in the previous process step. After development, an e-beam evaporation of a 10 nm Ni/400 nm Au metal stack was again performed and followed by a boiling-acetone lift-off. Nickel is used as an adhesion layer and the Au thickness is chosen to be equal to that of the metal via previously defined to ensure metal conformality. The final device is pictured in figure 7.

For variable-temperature measurements, a Janis cryostat is used and electrical measurements are made with an Agilent HP4145 controlled by in-house designed LabView software. Samples are bonded with a West Bond model 747677E wirebonder to a dip (Spectrum Semiconductor Materials, Inc.) using 1 mil gold wire.

3. Results and discussion

3.1. Overall device characteristics

We first sought to verify that the intrinsic NW material parameters could be extracted by comparing the resistance of

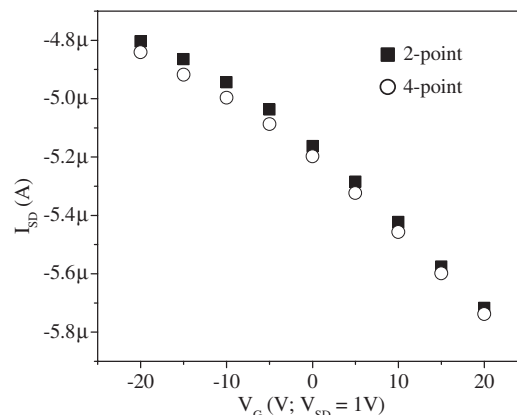


Figure 9. Two- and four-point $I_{SD}(V_{GD})$ sweeps illustrating that the transconductance is due only to change in the channel conductance.

the metal-semiconductor contacts to that of the NW. Fifty-one devices, each with four contacts, were measured at room temperature in both a two- and four-point configuration and the results are shown in figure 8. Devices from growths B, K, and L were used for this study because these wires were longer on average than other growths, thus many spanned four or more leads. The contribution from the contacts to the two-point resistance averages only 4.9% across the 51 devices, illustrating that the NW dominates electrical measurements. As will be shown, the carrier densities in these devices are sufficiently high for tunnelling Ohmics to be likely.

Four-point $I_{SD}(V_{SD}, V_{GD})$ measurements were performed to show that the observed transconductance is due to channel conductivity modulation and is not a contact effect. Figure 9 shows results comparing two-point and four-point carrier modulation for a representative device. There is little difference between the two- and four-point channel currents, eliminating the parasitic effects in the contact region for these devices.

We now consider electrical characteristics derived from FET results. In general, the FETs exhibit carrier densities in the $\sim 10^{20} \text{ cm}^{-3}$ range and mobilities in the $\sim 10 \text{ cm}^2 \text{ V}^{-1} \text{ s}^{-1}$ range. The devices show gating with monotonic $I_{SD}(V_{GD})$ dependences but saturation is not observed up to $V_{SD} = 15 \text{ V}$ (at which point the NWs are destroyed) due to the large carrier density. Even at these densities, however, some of the thinnest NW devices, all with diameters 25 nm or less, exhibit pinch-off, figure 10(a). It should be noted that pinch-off is not necessary for the accurate determination of material parameters. An $I_{SD}(V_{SD})$ sweep with V_{GD} varied is shown in figure 10(b) for the 10 nm diameter NW pictured in the SEM inset. This is one of the few devices, 14 out of 1096, that exhibited full pinch-off. The inset plot in figure 10(b) shows the I_{SD} dependence on V_{GD} when V_{SD} is held at 1 V (which yields a mobility of $9.49 \text{ cm}^2 \text{ V}^{-1} \text{ s}^{-1}$ and a carrier density of $1.62 \times 10^{20} \text{ cm}^{-3}$). The $I_{SD}(V_{SD})$ plot shows the Ohmic nature of the contacts as well as the fact that saturation is not reached, due to the high carrier densities of these NWs.

Variable temperature measurements are consistent with these carrier densities, exhibiting weak but monotonic dependences with temperature. The temperature dependence of the carrier concentration and mobility of a device from

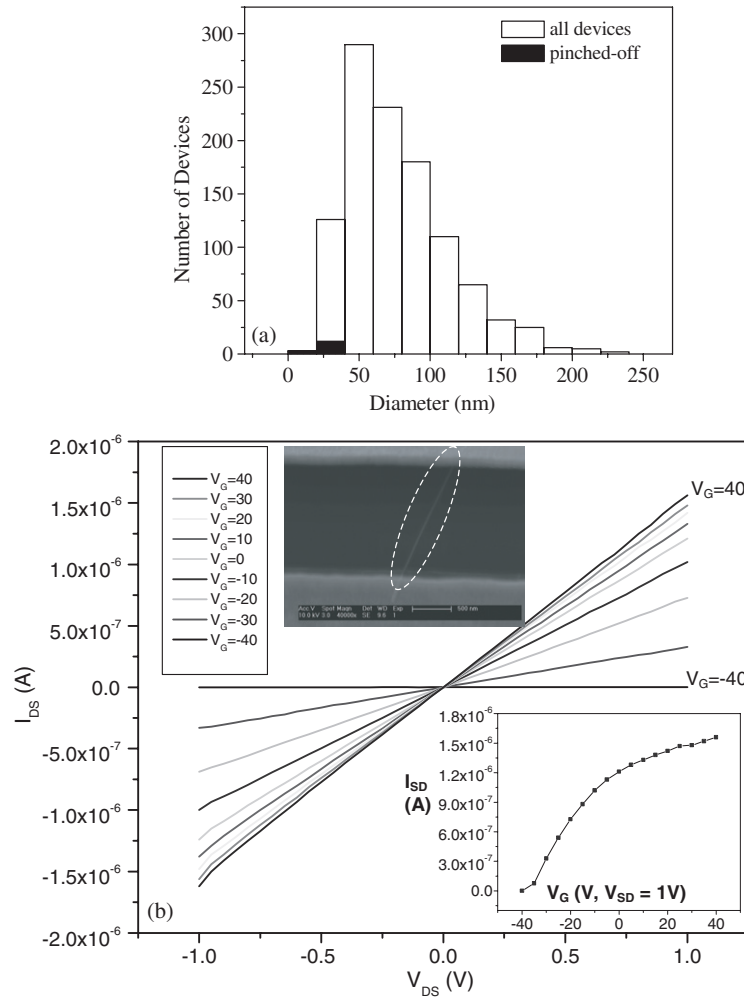


Figure 10. (a) A diameter histogram comparing the total number of devices from this study (1096), and the number exhibiting pinch-off (14). (b) An I_{SD} (V_{SD}) plot with V_{GD} varied for a 10 nm GaN device pictured in the inset (FE-SEM), one of the smallest measured. A gate voltage of -40 V is seen to turn the device off and that of 40 V to produce an $I_{SD} \sim 1.5 \mu\text{A}$ at $V_{SD} = 1$ V. The inset plot shows I_{SD} (V_{GD}) at $V_{SD} = 1$ V.

growth E is shown in figure 11. Overall, the temperature dependence of the conductance is minimal, decreasing by only 25% from room temperature and with a tendency to saturate below 120 K. It is observed that carrier concentration increases slightly with temperature above ~ 120 K, but the mobility shows a surprising decreasing trend for the same temperature range, consistent with phonon scattering processes rather than impurities. This behaviour is in agreement with the near-degenerate state indicated by the high carrier concentration ($\sim 10^{20} \text{ cm}^{-3}$) and was previously reported for GaN NWs [13].

Devices sometimes exhibit a small hysteresis in I_{SD} (V_{GD}) sweeps (with constant V_{SD}) for gate voltages $> |10 \text{ V}|$, the voltage range used in the transconductance determination. For 223 devices, the percentage error between transconductance values calculated from sweeps in opposite directions is $5.92 \pm 0.29\%$ ($\pm 1\sigma_M$, standard error of the mean). Thus, the total error reported for mobility and carrier concentration is the geometric mean of the error of the measurement error and the maximum due to potential hysteresis, 6.22%. In practice this turns out to be largely insignificant with respect to the other sources of error.

To verify that a statistically significant comparison can be performed to compare material synthesis parameters, we examine the fluctuations of intra-growth-run electrical characteristics and compare the electrical properties of NWs from two different fabrication runs with nominally identical growth parameters. The distribution of NW diameters for devices from growth run E (see table 1) is shown in figure 12(a); the mean diameter is 94.4 ± 3.5 ($1\sigma_M$) nm. Figures 12(b) and (c) are plots of carrier concentration (mean $\log n$ is 20.36 ± 0.03 ($1\sigma_M$) cm^{-3}) and mobility (mean mobility is 3.54 ± 0.28 ($1\sigma_M$) $\text{cm}^2 \text{ V}^{-1} \text{ s}^{-1}$) versus diameter for NW samples;² neither has a significant diameter dependence: for carrier density the coefficient of determination $R^2 = 0.20$, and for mobility $R^2 = 6.2 \times 10^{-4}$. Since the dispersion in device characteristics can both be interdevice and intradevice, a sampling of devices that had both a back-gate and multiple (>5) contacts were examined. Nanowire resistances derived from four-point measurements exhibit a 3.5% mean variation, and a 5.1% mean variation exists for mobilities and carrier

² Hereafter, mobility, carrier concentration, and diameter errors are reported as σ_M unless otherwise noted.

Table 2. Intradvice fluctuations for five devices with at least five successive contacts. The first and last leads for each device are the current source and sink, and resistances are reported for internal adjacent pairs. All geometrical parameters are the same for each pair. Resistance values are derived from the inverse of the best-fit line to a four-point I - V sweep. The deviation $\overline{\Delta R}/\overline{R}$ (%) is determined from the means of the variances divided by the mean of the average.

Lead pair	Device 1	Device 2	Device 3	Device 4	Device 5
A	70 320 Ω	889 846 Ω	40 783 Ω	289 733 Ω	32 164 Ω
B	70 849 Ω	873 489 Ω	42 089 Ω	294 654 Ω	33 481 Ω
C	NA	NA	40 142	272 228 Ω	33 051 Ω
D	NA	NA	NA	NA	31 034 Ω
E	NA	NA	NA	NA	31 744 Ω
$\overline{\Delta R}/\overline{R}$ (%)	0.75	1.86	3.97	4.79	3.46

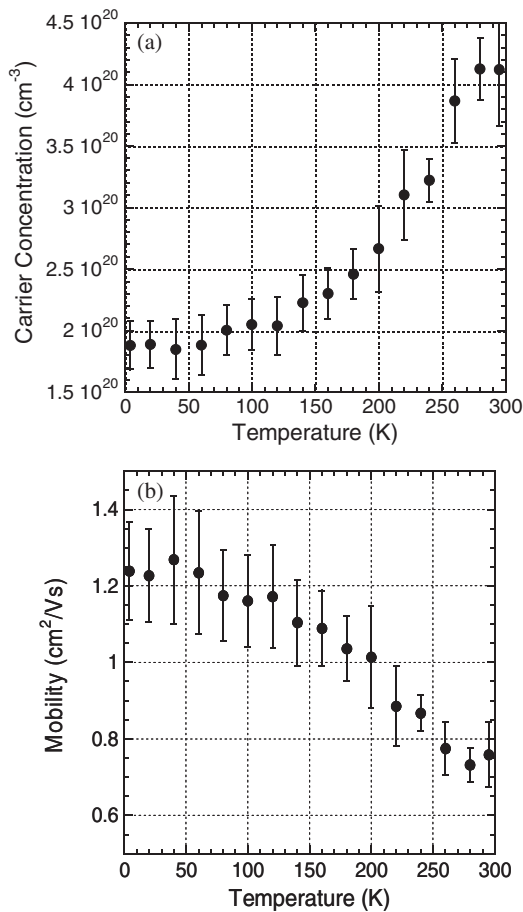


Figure 11. Temperature dependence of the extracted carrier concentration (a) and mobility (b) for growth E.

concentrations between different leads contacting the same wire (table 2). Thus, interdevice fluctuations dominate over intradvice variances. Reported values of mobility and carrier concentration do not include this error (by geometric mean of the errors) since the sample size of multiple-point devices is sparse; however, the correction is insignificant.

A second sample was grown under nominally identical conditions (sample D), with the following comparison: the mean mobility for D is $2.96 \pm 0.36 \text{ cm}^2 \text{ V}^{-1} \text{ s}^{-1}$, and that for E is $3.54 \pm 0.28 \text{ cm}^2 \text{ V}^{-1} \text{ s}^{-1}$. The mean log carrier concentration for D is $20.43 \pm 0.05 \text{ cm}^{-3}$ and that for E is $20.36 \pm 0.03 \text{ cm}^{-3}$. A plot of mobility versus the log of the carrier concentration for both samples D and E is shown in figure 12(d). Population means (triangle) $\pm 1\sigma_M$

(brackets) are shown at the periphery of the plot. Brackets are not observable when the $\pm 1\sigma_M$ range is less than the width of the data point (triangle) signifying the mean. A T -test is performed to compare the sample populations and to assess the significance of population isolation. At the 95% confidence level (CL), neither the mobility nor the carrier concentration is statistically different. Thus, populations with nominally identical growth conditions yield statistically identical mobilities and carrier densities.

Since the back-gated geometry is essential for the high throughput characterization required for NW material optimization, the use of a back-gate in place of a traditional top-gate was validated by employing e-beam lithography to define a top-gate over an optically contacted NW from growth E. Sweeps of I_{SD} (V_{SD}) with V_{GD} varied from -40 to 40 V in 10 V steps are shown in figure 13(a) for the device pictured in figure 7 for both the top-gate and the back-gate. As expected, the current level of the device when top-gated is slightly higher, due to the narrower gate. Figure 13(b) shows the I_{SD} (V_{GD}) plots at $V_{SD} = 1 \text{ V}$ for both gates, illustrating no appreciable difference in transconductance.

3.2. Growth parameter study

The previous section has established that the method for extracting material parameters is valid, intra- and inter-device fluctuations can be quantified, and that growth parameters can be statistically compared. Thus, we can now examine the effects of changing growth parameters on electrical characteristics. As discussed previously, the seven adjustable growth parameters in the HW-CVD system are listed for each sample in table 1.

We first sought to decrease the diameter of the NWs. This was attempted by changing the substrate because wire diameter is dependent on catalyst size, which in turn is dependent on metal atom diffusion mobility on the substrate. A comparison of the diameters of NWs grown on alumina (growth A) with ones grown on Si (growth B) with all other growth parameters held equal is shown in figure 14(a). The wires fabricated and measured from growth A average $125.36 \pm 3.4 \text{ nm}$ in diameter compared with an average diameter for growth B of $62.7 \pm 3.0 \text{ nm}$. T -test results show the diameters to be different at the 99.9% CL, with $t = 9.80$, $p = 4.34 \times 10^{-17}$.³ Thus, switching to a Si substrate effectively decreases NW diameter.

³ In a T -test, the t -value is the ratio of the difference between the population means to the standard error of the mean, defined as $t = \frac{\bar{X}_T - \bar{X}_C}{\sqrt{\frac{\text{var}_T}{n_T} + \frac{\text{var}_C}{n_C}}}$. The p -value is the two-tailed probability computed using a t -distribution, with smaller values representing greater population separations.

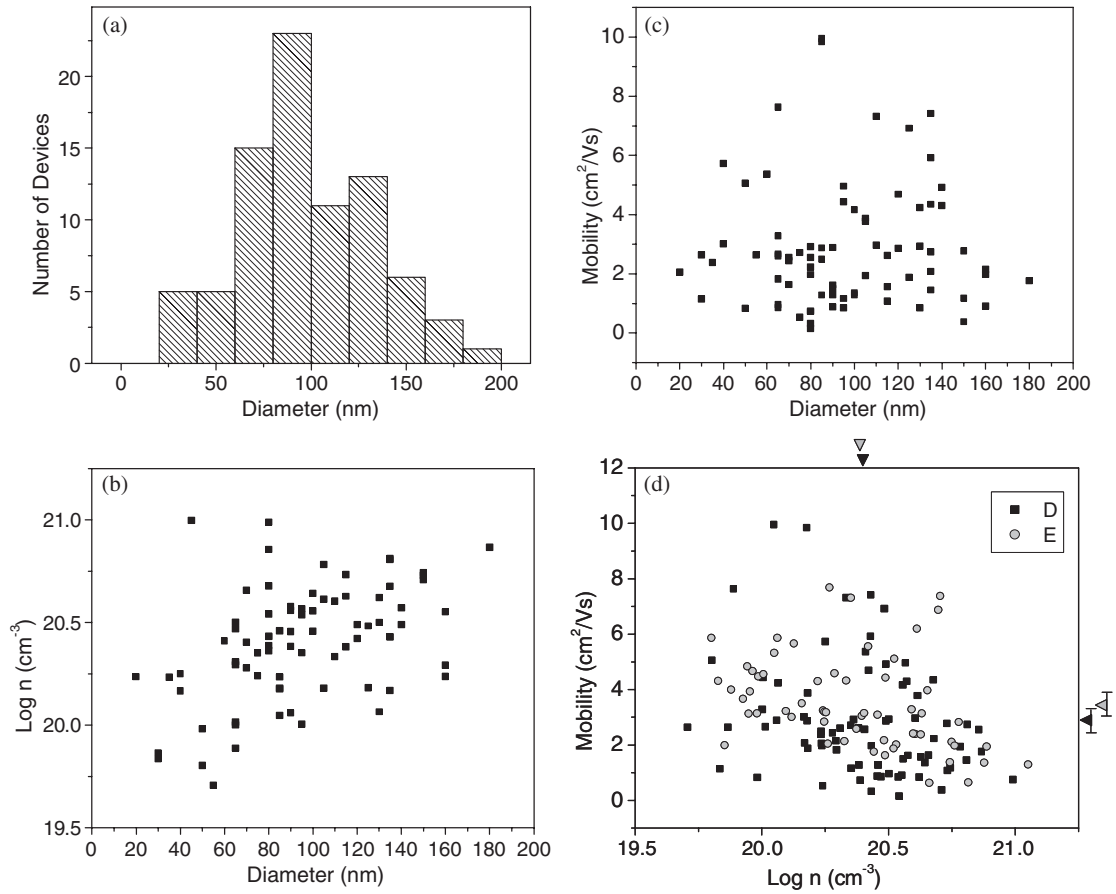


Figure 12. (a) Diameter histogram for NW sample E (see table 1). The mean diameter is 94.4 ± 3.5 nm. (b) Plot of \log carrier concentration versus diameter for growth E. The mean $\log n$ is 20.36 ± 0.03 cm^{-3} . (c) Plot of mobility versus diameter for growth E. The mean mobility is 3.54 ± 0.28 $\text{cm}^2 \text{V}^{-1} \text{s}^{-1}$. (d) Comparison of growths D and E. The mean mobility for D is 2.96 ± 0.36 $\text{cm}^2 \text{V}^{-1} \text{s}^{-1}$ and its mean $\log n$ is 20.43 ± 0.05 cm^{-3} . The T -test results for mobility are not significantly different at 95% confidence level (CL), $t = 1.59$, $p = 0.11$; and for carrier concentration not significantly different at the 95% confidence level (CL), $t = 1.24$, $p = 0.21$. The means (with $1\sigma_M$ error bars) are displayed on the periphery of the graph, and are consistent with this observation.

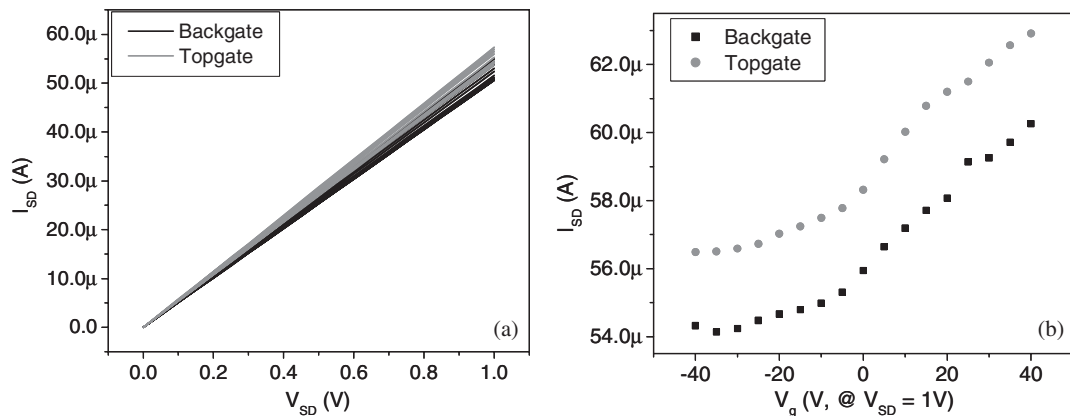


Figure 13. (a) I_{SD} (V_{SD}) sweeps with V_{GD} varied from -40 to 40 in 10 V increments. The black curve shows the back-gate and the grey shows the top-gate as the gate electrode. (b) A plot of I_{SD} (V_{GD}) at $V_{SD} = 1$ V for the back-gate (black) and top-gate (grey).

Changing substrates from alumina to Si was also found to decrease mobility from 6.43 ± 0.52 $\text{cm}^2 \text{V}^{-1} \text{s}^{-1}$ to 4.84 ± 0.41 $\text{cm}^2 \text{V}^{-1} \text{s}^{-1}$ (99.9% CL, $t = 3.48$, $p = 7.10 \times 10^{-4}$) and to decrease \log doping density from 20.20 ± 0.03 cm^{-3} to 19.89 ± 0.03 cm^{-3} (99.9% CL, $t = 3.86$, $p = 2.42 \times 10^{-12}$),

as shown in figure 14(b). Thus, a Si substrate is preferred over alumina both for reducing diameter and lowering doping density, though mobility suffers. A comparison of NWs grown on an alumina substrate lying flat (growth C) to those from the upright alumina template of growth A showed that

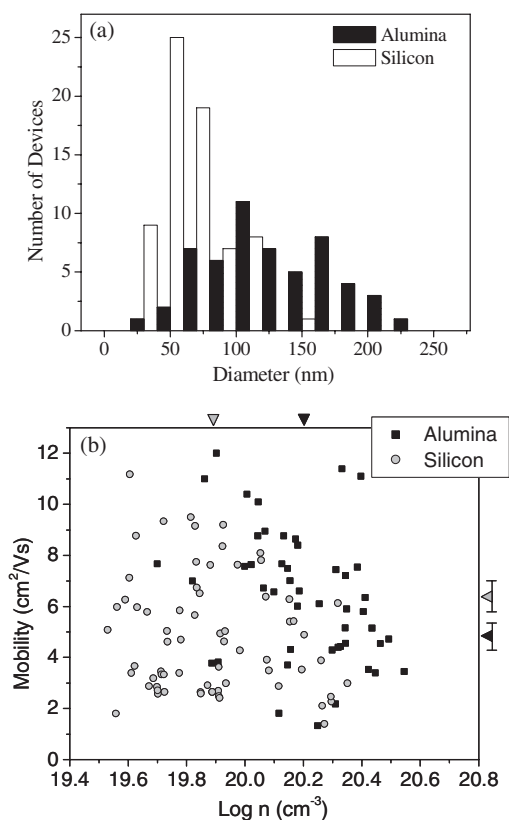


Figure 14. (a) Diameter histogram for growths A (alumina) and B (silicon). The average diameter for A is 125.36 ± 3.4 nm and for B is 62.4 ± 3.0 nm. *T*-test results: significantly different at 99.9% CL ($t = 9.80$, $p = 4.34 \times 10^{-17}$). (b) Plot of mobility versus $\log n$ for A and B. The mean $\log n$ for A is 20.20 ± 0.03 cm^{-3} and the mean mobility is 6.43 ± 0.52 $\text{cm}^2 \text{V}^{-1} \text{s}^{-1}$. The mean $\log n$ for B is 19.89 ± 0.03 cm^{-3} and the mean mobility is 4.83 ± 0.41 $\text{cm}^2 \text{V}^{-1} \text{s}^{-1}$. *T*-test results: mobility, significantly different at 99.9% level, $t = 3.60$, $p = 4.61 \times 10^{-4}$; carrier concentration, significantly different at 99.9% level, $t = 7.86$, $p = 2.42 \times 10^{-12}$.

sample orientation had negligible effects on mobility and carrier concentration.

We next sought to change the two most straightforward growth parameters, the temperature and pressure of the furnace during growth. Growth temperatures were increased in 100°C increments from 800 to 1100°C —growths J, B, K, and L, respectively—and electrical characteristics of the resulting NWs were measured, as shown in figure 15(a). The mean mobility for J is 5.54 ± 0.46 $\text{cm}^2 \text{V}^{-1} \text{s}^{-1}$, that for B is 4.83 ± 0.41 $\text{cm}^2 \text{V}^{-1} \text{s}^{-1}$, that for K is 7.36 ± 0.79 $\text{cm}^2 \text{V}^{-1} \text{s}^{-1}$, and that for L is 6.87 ± 0.69 $\text{cm}^2 \text{V}^{-1} \text{s}^{-1}$, and the mean \log carrier density for J is 20.27 ± 0.02 cm^{-3} , that for B is 19.89 ± 0.03 cm^{-3} , that for K is 19.95 ± 0.03 cm^{-3} , and that for L is 19.79 ± 0.04 cm^{-3} . The mobilities of the temperature extremes, growths J and L, are significantly different at the 95% level but not the 99% level, with $t = 2.20$ and $p = 0.03$. At the 99.9% confidence level the carrier concentrations of these samples are significantly different, with $t = 11.42$ and $p = 2.17 \times 10^{-20}$. Thus increasing temperature produces wires with slightly better (lower n , higher μ) electronic properties. It should be noted that this is not a strict dependence; for example, the mean carrier density for growth K is higher than growth

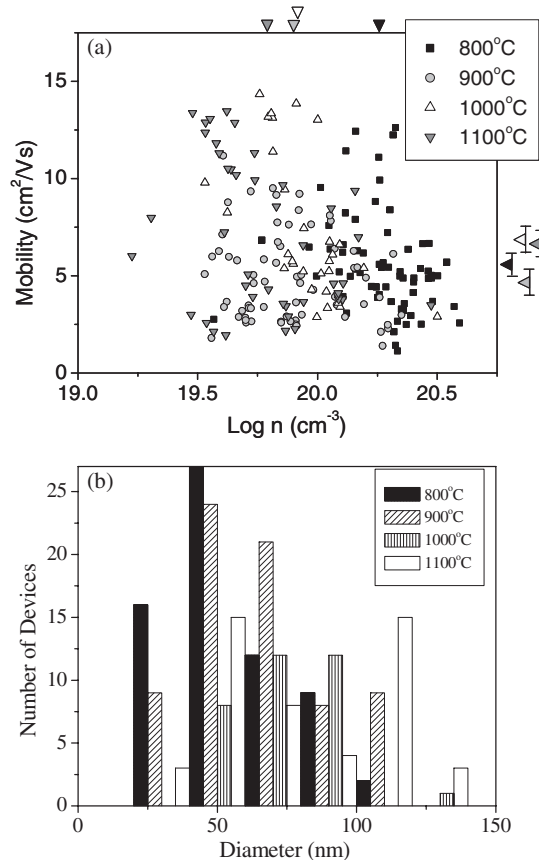


Figure 15. (a) Plot of mobility versus $\log n$ for three growths at different temperatures: 800°C (I), 900°C (B), 1000°C (J), 1100°C (K). The mean mobility for J is 5.54 ± 0.46 $\text{cm}^2 \text{V}^{-1} \text{s}^{-1}$, that for B is 4.83 ± 0.41 $\text{cm}^2 \text{V}^{-1} \text{s}^{-1}$, that for K is 7.36 ± 0.79 $\text{cm}^2 \text{V}^{-1} \text{s}^{-1}$, and that for L is 6.87 ± 0.69 $\text{cm}^2 \text{V}^{-1} \text{s}^{-1}$, and the mean \log carrier density for J is 20.27 ± 0.02 cm^{-3} , that for B is 19.89 ± 0.03 cm^{-3} , that for K is 19.95 ± 0.03 cm^{-3} , and that for L is 19.79 ± 0.04 cm^{-3} . The mobilities of the temperature extremes, growths J and L, are significantly different at the 95% level but not the 99% level, where $t = 2.20$ and $p = 0.03$. At the 99.9% CL the carrier concentrations of these samples are significantly different, with $t = 11.42$ and $p = 2.17 \times 10^{-20}$. (b) Diameter histogram for growths J, B, K, and L. The mean diameter for J is 53.4 ± 2.3 nm, that for B is 62.4 ± 2.7 nm, that for K is 70.8 ± 2.6 nm, and that for L is 77.1 ± 4.2 nm.

B, though it occurred at a higher temperature. Comparing diameters of NWs from these growths, figure 15(b), we observe that increased temperature produces thicker wires: the mean diameter for J is 53.4 ± 2.3 nm, that for B is 62.4 ± 2.7 nm, that for K is 70.8 ± 2.6 nm, and that for L is 77.1 ± 4.2 nm. This is understood by increased catalyst mobility at higher temperatures, which produces larger catalyst nanoparticles and, in turn, thicker wires. It is also interesting to note that NWs grown at the higher temperatures (1000 and 1100°C) were generally much longer; this could be indicative that the NW is a kinetically, rather than a thermodynamically, stable structure which is favoured at higher temperatures.

All growths described to this point occurred at 760 Torr. Successful growths have been performed at pressures down to 70 Torr, although NW yield is found to be greatly reduced at pressures lower than 300 Torr. A growth performed at 300 Torr

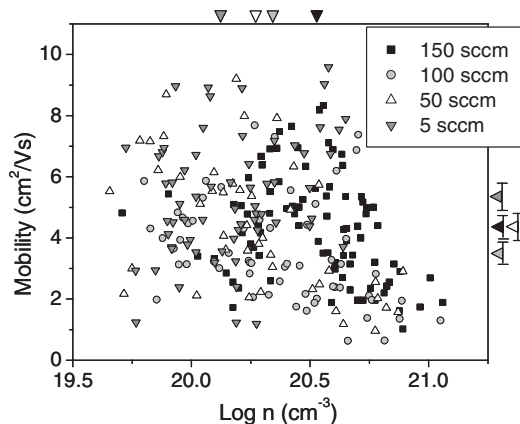


Figure 16. Plot of mobility versus $\log n$ for four growths with different NH_3 flows: 150 sccm (F), 100 sccm (D), 50 sccm (G), and 5 sccm (H). The mean mobilities for F, D, G, and H, respectively, are $4.32 \pm 0.32 \text{ cm}^2 \text{ V}^{-1} \text{ s}^{-1}$, $2.96 \pm 0.36 \text{ cm}^2 \text{ V}^{-1} \text{ s}^{-1}$, $4.39 \pm 0.41 \text{ cm}^2 \text{ V}^{-1} \text{ s}^{-1}$, and $5.42 \pm 0.41 \text{ cm}^2 \text{ V}^{-1} \text{ s}^{-1}$; the mean \log carrier concentrations, respectively, are $20.52 \pm 0.03 \text{ cm}^{-3}$, $20.43 \pm 0.05 \text{ cm}^{-3}$, $20.27 \pm 0.05 \text{ cm}^{-3}$, and $20.17 \pm 0.03 \text{ cm}^{-3}$. For F versus D: the mobilities are significantly different at the 95% CL but not at the 99% level, where $t = 2.59$ and $p = 0.01$; the carrier density is statistically different at the 99.9% CL with $t = 4.09$ and $p = 7.14 \times 10^{-3}$. For G versus D: the mobilities are significantly different at the 95% CL but not at the 99% level, where $t = 2.29$ and $p = 0.02$, and the carrier densities are not statistically different at the 95% CL with $t = 0.27$ and $p = 0.79$. For G versus H: the mobilities are not significantly different at the 95% CL, where $t = 1.60$ and $p = 0.11$, and the carrier densities are statistically different at the 95% CL but not at the 99% level with $t = 2.30$ and $p = 0.02$.

(growth N) with suitable yield for fabrication was compared with a growth at 760 Torr (growth M). At the 95% CL neither the mobilities nor the carrier concentrations were significantly different; thus in this high-pressure range, changes in pressure are seen to have a negligible effect on electronic parameters.

Since the intrinsic doping of as-grown GaN is due to either nitrogen vacancies or oxygen impurities, we postulated that altering the ammonia flux could change the incorporated nitrogen rate and, in turn, potentially decrease the carrier concentration. The flow rate of ammonia was varied from 5 to 150 sccm (growths E, F, G, and H), and the mobility versus \log carrier density is shown in figure 16. The carrier density was found to have only a weak dependence, tending to decrease slightly with decreasing flow, and a >99% CL correlation was not observed.

We surmised that oxygen impurities, the alternative doping mechanism to nitrogen vacancies, were produced by the presence of Ga_2O_3 in the growth furnace. At high temperature,



Gallium (I) oxide has a vapour pressure four orders of magnitude higher than Ga (1.0 Torr versus 1×10^{-4} Torr at 900°C), thus it increases the Ga flux in the furnace during growth. In order to ascertain if the oxygen due to the presence of gallium oxide was being incorporated as an NW dopant, growth I was performed without Ga_2O_3 . The average mobility for NWs from this growth is $6.38 \pm 0.68 \text{ cm}^2 \text{ V}^{-1} \text{ s}^{-1}$ (compared with $3.54 \pm 1.69 \text{ cm}^2 \text{ V}^{-1} \text{ s}^{-1}$ for growth A) and

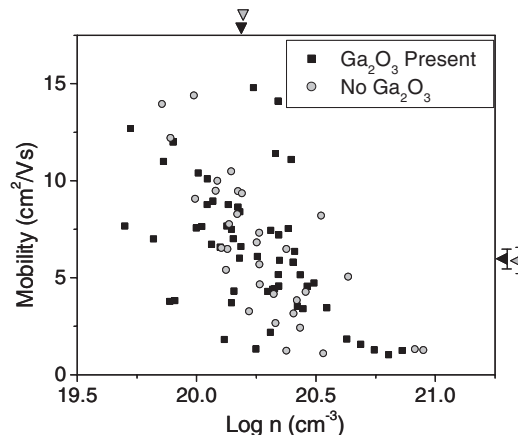


Figure 17. Plot of mobility versus $\log n$ for a sample grown with Ga + Ga_2O_3 (A) and one grown with only Ga as the Ga source (H). The average mobility for NWs for H is $6.38 \pm 0.68 \text{ cm}^2 \text{ V}^{-1} \text{ s}^{-1}$ (compared with $3.54 \pm 1.69 \text{ cm}^2 \text{ V}^{-1} \text{ s}^{-1}$ for A) and the average \log carrier concentration is $20.24 \pm 0.04 \text{ cm}^{-3}$ (compared with $20.20 \pm 0.03 \text{ cm}^{-3}$ for A). At the 95% CL neither the mobilities, $t = 0.03$ and $p = 0.98$, nor the carrier concentrations, $t = 0.69$ and $p = 0.49$, are significantly different.

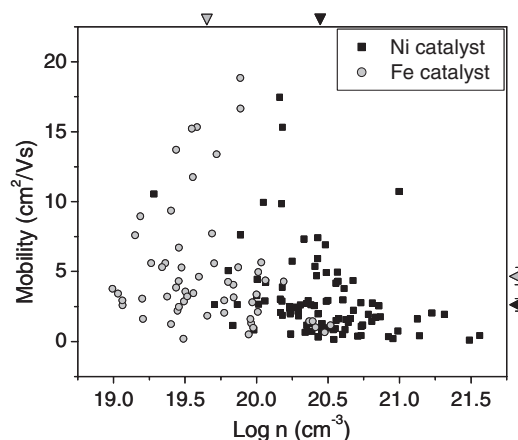


Figure 18. Plot of mobility versus $\log n$ for a sample grown with a Ni catalyst (M) and one grown with an Fe catalyst (O). The mean mobility for growth M is $4.82 \pm 0.59 \text{ cm}^2 \text{ V}^{-1} \text{ s}^{-1}$ and that for growth O is $2.73 \pm 0.30 \text{ cm}^2 \text{ V}^{-1} \text{ s}^{-1}$; the mean \log carrier density for M is $19.63 \pm 0.05 \text{ cm}^{-3}$ and that for O is $20.44 \pm 0.03 \text{ cm}^{-3}$. At the 99% CL the mobilities are significantly different but not at the 99.9% level, where $t = 3.21$ and $p = 0.002$. At the 99.9% level the carrier concentrations are significantly different with $t = 12.63$ and $p = 2.61 \times 10^{-25}$.

the average \log carrier concentration is $20.24 \pm 0.04 \text{ cm}^{-3}$ (compared with $20.20 \pm 0.03 \text{ cm}^{-3}$ for growth A), figure 17. At the 95% CL neither the mobilities nor the carrier concentrations are significantly different. Thus, it was found that the presence of oxygen due to Ga_2O_3 does not significantly affect the electrical quality of the NWs.

Using Fe as a catalyst has been reported to produce GaN NWs with significantly greater mobilities and lower carrier densities [15]. Growths M (Fe catalyst) and O (Ni catalyst) compare these catalysts and the results are shown in figure 18. It should be noted that growths with Fe catalysts produce nominally lower NW yields as compared with Ni. The mean mobility for growth M is $4.82 \pm 0.59 \text{ cm}^2 \text{ V}^{-1} \text{ s}^{-1}$ and that

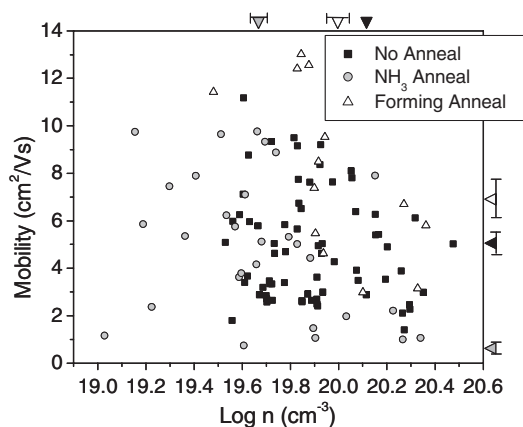


Figure 19. Plot of mobility versus $\log n$ for a sample annealed in forming gas (S) and a different sample from the same growth annealed in NH_3 (R) compared with an unannealed one from a different growth with nominally identical growth conditions (B). The mean mobilities of samples B, S, and R are 4.83 ± 0.41 , 7.96 ± 1.02 , and $5.01 \pm 0.61 \text{ cm}^2 \text{ V}^{-1} \text{ s}^{-1}$, respectively; the mean log carrier concentrations of the samples in the same order are 19.89 ± 0.03 , 19.98 ± 0.06 , and $19.67 \pm 0.06 \text{ cm}^{-3}$. At the 99.9% CL the ammonia anneal decreases the carrier concentration ($t = 3.84$, $p = 2.44 \times 10^{-4}$) while the forming gas anneal does not produce a significantly different carrier concentration at the 95% CL ($t = 1.19$, $p = 0.24$).

for growth O is $2.73 \pm 0.30 \text{ cm}^2 \text{ V}^{-1} \text{ s}^{-1}$; the mean log carrier density for M is $19.63 \pm 0.05 \text{ cm}^{-3}$ and that for O is $20.44 \pm 0.03 \text{ cm}^{-3}$. At the 99% CL the mobilities are significantly different and the carrier concentrations are significantly different at the 99.9% level ($t = 12.63$, $p = 2.61 \times 10^{-25}$). Thus, the Fe catalyst greatly decreases the NW carrier concentration, though the average concentration, $4.65 \times 10^{19} \text{ cm}^{-3}$, is still in the near-degenerate region. The potential incorporation of oxygen as a dopant via the presence of Ga_2O_3 was also investigated with Fe-catalyst NWs (growths P and Q), and, as with Ni, no significant difference in carrier density was observed.

Since free oxygen is not being incorporated as a dopant, a test for nitrogen vacancies as the dopant was devised. Previously it was observed there was no significant dependence on the ammonia flow during growth, indicating that little could be done to affect nitrogen incorporation during growth. This led us to select a post-growth, pre-fabrication anneal of the NWs in (atomic) nitrogen, which was calculated (using bulk parameters) to have sufficient diffusivity to potentially fill these vacancies. Nanowires from the same growth were annealed at 900°C in either forming gas (4% H_2 in N_2) or ammonia, and compared to a sample grown with nominally identical conditions with no anneal (growth B), figure 19. The forming gas anneal (growth S) does not produce atomic nitrogen and, in turn, should have a minimal effect on NW quality, while nitrogen produced by the ammonia cracking during this anneal (growth R) should decrease the carrier concentration. The mean mobilities of samples B, S, and R are 4.83 ± 0.41 , 7.96 ± 1.02 , and $5.01 \pm 0.61 \text{ cm}^2 \text{ V}^{-1} \text{ s}^{-1}$, respectively; the mean log carrier concentrations of the samples in the same order are 19.89 ± 0.03 , 19.98 ± 0.06 , and $19.67 \pm 0.06 \text{ cm}^{-3}$. At the 99.9% CL the ammonia anneal decreases the carrier

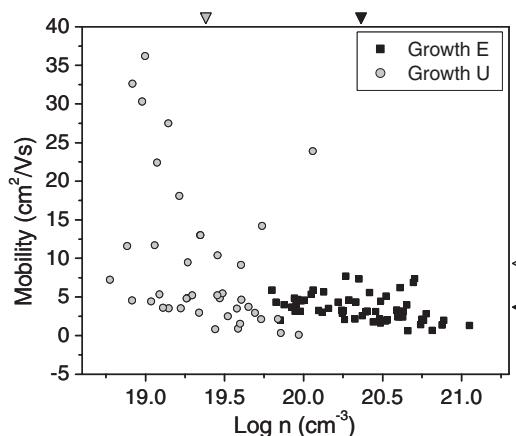


Figure 20. Plot of mobility versus $\log n$ for a sample with optimized growth conditions (U) versus the original sample grown with non-optimized conditions (E). The average mobility for U is $9.12 \pm 1.56 \text{ cm}^2 \text{ V}^{-1} \text{ s}^{-1}$ (versus $3.54 \pm 0.28 \text{ cm}^2 \text{ V}^{-1} \text{ s}^{-1}$ for E) and the mean log carrier density is $19.39 \pm 0.05 \text{ cm}^{-3}$ (versus $20.36 \pm 0.03 \text{ cm}^{-3}$). The mobilities and carrier concentrations are each significantly different at the 99.9% CL with $t = 4.48$, $p = 2.04 \times 10^{-5}$ and $t = 15.58$, $p = 2.87 \times 10^{-28}$, respectively.

concentration ($t = 3.84$, $p = 2.44 \times 10^{-4}$) while the forming gas anneal does not produce a significantly different carrier concentration at the 95% CL. Thus, nitrogen vacancies are found to be the dominant as-grown n-type intrinsic dopant in these NWs.

3.3. Optimization

Combining the results of the above studies, one can optimize material parameters for higher mobility and lower carrier concentration. For growths T and U, Si was chosen as the substrate and Fe as the catalyst, the ammonia flux was set at 2 sccm, a high temperature— 950°C —and atmospheric pressure were used, and Ga and Ga_2O_3 were used (to increase yield). One of the substrates, U, was then annealed in NH_3 for 4 h at 900°C , the same conditions as growth S. The anneal was found to increase the mobility while decreasing the carrier concentration. The average mobility for the annealed sample is $9.12 \pm 1.56 \text{ cm}^2 \text{ V}^{-1} \text{ s}^{-1}$ and the mean log carrier density is $19.39 \pm 0.05 \text{ cm}^{-3}$. Further, the NWs of growth U show significant improvement in parameters necessary for electronic devices over the non-optimized growth parameters commonly found in the literature [16] for GaN HW-CVD NWs. A comparison of U to the original growth conditions (E) shows a stark contrast in both mobility and carrier concentration, seen in figure 20.

4. Conclusions

We demonstrate here a procedure to effectively optimize electronic material parameters for semiconducting nanowires. For the specific HW-CVD GaN system we have determined that nitrogen vacancies are the dominant dopant responsible for intrinsic n-doping. The method is applicable to any NW (or mesoscopic) electronic device and relies upon a statistically significant number of devices. We were also able to distinguish between intradevice and interdevice fluctuations, finding that interdevice fluctuations dominate the observed fluctuations.

Acknowledgments

We would like to thank Professor Jung Han and Dr George Cui for assistance in furnace implementation, Dr Luigi Frunzio, Christopher Tillinghast, and Matthew Reese for fabrication suggestions, Dr Ling Xie and John Tsakirgis for their processing help in the Harvard University NNIN Cleanroom, and Dr Zhenting Jiang for help with FE-SEM microscopy. This work was partially supported by DARPA under SPAWAR contract number N66001-04-1-8902, ARO (DAAD19-01-1-0592), AFOSR (F49620-01-1-0358), NASA (NCC 2-1363), by the Department of Homeland Security, and by the National Science Foundation.

References

- [1] Wagner R S 1970 *Whisker Technology* ed A P Levitt (New York: Wiley) pp 47–109
- [2] Hiruma K, Yazawa M, Katsuyama T, Ogawa K, Haraguchi K, Koguchi M and Kakibayashi H 1995 *J. Appl. Phys.* **77** 447
- [3] Björk M T, Ohlsson B J, Sass T, Persson A I, Thelander C, Magnusson M H, Deppert K, Wallenberg L R and Samuelson L 2002 *Appl. Phys. Lett.* **80** 1058
Björk M T, Ohlsson B J, Thelander C, Persson A I, Deppert K, Wallenberg L R and Samuelson L 2002 *Appl. Phys. Lett.* **81** 4458
- [4] Gudiksen M S, Lauhon L J, Wang J, Smith D C and Lieber C M 2002 *Nature* **415** 617
Huang Y, Duan X F and Lieber C M 2005 *Small* **1** 142
- [5] Kuykendall T, Pauzauskie P, Lee S, Zhang Y, Goldberger J and Yang P 2003 *Nano Lett.* **3** 1063
- [6] Poole P J, Lefebvre J and Fraser J 2003 *Appl. Phys. Lett.* **83** 2055
- [7] Wu Z H, Mei X, Kim D, Blumin M, Ruda H E, Liu J Q and Kavanagh K L 2003 *Appl. Phys. Lett.* **83** 3368
- [8] Han S, Jin W, Tang T, Li C, Zhang D H, Liu X L, Han J and Zhou C W 2003 *J. Mater. Res.* **18** 245
- [9] Cheng G, Kolmakov A, Zhang Y, Moskovits M, Munden R, Reed M A, Wang G, Moses D and Zhang J 2003 *Appl. Phys. Lett.* **83** 1578
- [10] Givargizov E I 1975 *J. Cryst. Growth* **31** 20
- [11] Seifert W *et al* 2004 *J. Cryst. Growth* **272** 211
- [12] Shi W, Zheng Y, Wang N, Lee C-S and Lee S-T 2001 *Adv. Mater.* **8** 591
- [13] Kim J-R, Kim B-K, Lee I J, Kim J-J, Kim J, Lyu S C and Lee C J 2004 *Phys. Rev. B* **69** 233303
- [14] Stern E, Cheng G, Li C, Klemic J, Broomfield E, Turner-Evans D, Zhou C and Reed M A 2005 Methods for fabricating Ohmic contacts to nanowires and nanotubes submitted
- [15] Huang Y, Duan X, Cui Y and Lieber C M 2002 *Nano Lett.* **2** 101
- [16] Kim J-R, So H M, Park J W, Kim J-J, Kim J, Lee C J and Lyu S C 2002 *Appl. Phys. Lett.* **80** 3548